# Precision Landing for Fixed-wing UAV using Ultra-Wide-Band Ranging

Gautier Hattenberger*

ENAC, University of Toulouse, France

## ABSTRACT

Fixed-wing mini UAVs usually require a large area in order to safely land, eventually directly using the fuselage body as a landing skid. In some cases, the ground surface is not suitable for this type of operation and may damage the aircraft. A common option is to use a net to capture the plane, but the GPS accuracy may not be sufficient to allow a reliable landing in full autonomy. In this paper, we are investigating the use of Ultra-Wide-Band communication modules, used as ranging systems, in order to determine the position of the UAV during its final approach. This information is then used to adjust the trajectory towards the landing net. The focus is made to the calibration procedure, the data fusion Kalman filter to estimate the position of the UAV and the overall performances of the system.

## 1 INTRODUCTION

Fixed-wing mini Unmanned-Aerial-Vehicles (UAV) usually require a large area in order to safely land, eventually directly using the fuselage body as a landing skid. In some cases, the ground surface is not suitable for this type of operation and may damage the aircraft. A common option is to use a net to capture the plane, as seen on Figure 1, but the GPS accuracy may not be sufficient to allow a reliable landing in full autonomy.

Several solutions for precision landing of aircraft are available, mostly relying on vision [1, 2] or Differential-GPS (DGPS). Solutions based on vision usually require an higher computational power and sensors (cameras) that may not be adapted to flights in harsh conditions (such as inside clouds for meteorological studies). DGPS is rather easy to use but can be a bit more expensive. Radar and Lidar are not considered since this type of sensors are most of the time too heavy and expensive to be used on light UAVs. An other popular technology is to use Ultra-Wide-Band (UWB) communication devices that can also provide accurate range measurements [3]. This approach have been already successfully applied on UAVs, eventually in combination with other sensors [4, 5].

The principle of localization based on distance measurements rely on algorithms called trilateration or multilateration

---

*gautier.hattenberger@enac.fr



Figure 1: Fleet of UAVs for meteorological studies in harsh and remote location. A net is required to land the planes. Courtesy of Greg Roberts from French Meteorological Research Center.

depending on the number of measurements [6]. The position can be extracted by direct computation or by using linear algebra like Singular-Value Decomposition or Bayesian filters such as Kalman filters [7, 8].

After describing the parametrization and the reference frame used in this article, the next section will present the trilateration direct method and evaluate its performances for localization of a UAV. Then, based on experimental data, a solution using an Extended Kalman Filter for continuous integration is proposed, eventually taking the turn rate into account to reduce the latency.

## 2 PROBLEM STATEMENT

In order to build a coordinate frame local to the landing net that would be easy to install for the UAV operators, a first assumption is made on the placement of the anchors used for distance measurements. As it will be shown in section 3.2, a minimum of three anchors are required for this localization problem. If we consider a plane landing at the position (0,0) in a direction facing the $x$ axis, the Figure 2 is showing the situation (top view, $xy$ being the horizontal plane). Each anchor is measuring a distance ($d1$, $d2$ or $d3$) to the plane equipped with a fourth module configured as a tag. The relative positions of the anchors are defined by a lateral separation $d_{lat}$ between anchors 2 and 3 symmetrical along the $y$ axis, and a longitudinal distance to the origin $d_{lon}$ of the third one along the $x$ axis.

The desired landing path for a typical mini UAV of 1 me-

  
**IMAV2018-30**

http://www.imavs.org/pdf/imav.2018.30

10th International Micro-Air Vehicles Conference
22nd-23rd November 2018. Melbourne, Australia.
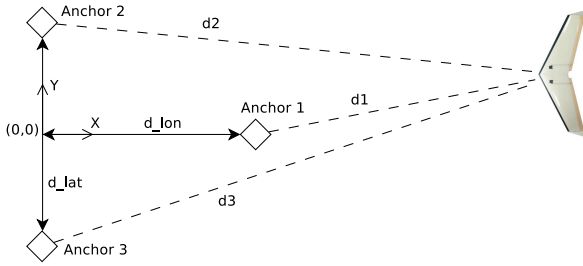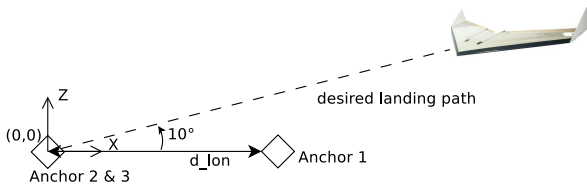
Figure 2: Three anchors and the local coordinate frame.

ter wingspan with a flight speed around 15 m/s is a slope $\gamma_{land} = 10°$, as depicted on Figure 3. This reference path will be used later for the theoretical precision evaluation in section 3.3.

Figure 3: Desired landing path with an angle of 10°.

## 3 LOCALIZATION BASED ON RANGING

### 3.1 Calibration of the ranging devices

A first step to localization is the calibration and the performance evaluation of the ranging devices. In this study, the *DW1000M* modules from *Decawave*[1] have been used. According to the datasheet, the ranging accuracy is 10 cm, with a maximum distance around 200 meters in direct line of sight. It has been measured up to 250 meters by setting the transmitter and receiver power to the maximum. The calibration process consists in comparing the distances reported by two modules (an anchor and a tag) with ground references placed every 10 meters (up to 100 meter) and match the data with the model $distance = scale * raw - offset$. The result presented Figure 4 clearly shows the excellent correlation of the measured data other the references. In addition, the standard deviation is stable for all distances with an average $\sigma_{avr} = 0.026$, which means that most of the measures (in the range $3\sigma$) are less than 10 cm.

The Table 1 gives the calibration of the three anchors against the tag module. As expected, the scale factors are all close to 1, and the offsets are all less than 1 meter.

### 3.2 Direct position from trilateration or multilateration

The method used to determine the 3D position of the tag based on distances will depend on the number of anchors $N$,
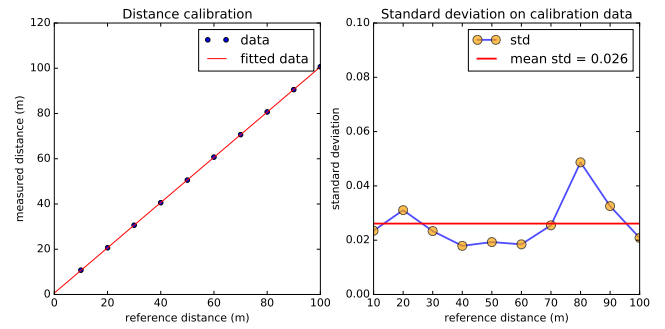
[1]http://www.decawave.com

Figure 4: Calibration points and standard deviation of a DW1000 module.

| anchor | scale | offset (in meter) |
|--------|--------|-------------------|
| 1 | 0.9999 | 0.6389 |
| 2 | 0.9972 | 0.9027 |
| 3 | 0.9979 | 0.8506 |

Table 1: Calibration results for the three anchors against the tag module.

assuming that they respect certain constraints.

- If $N = 3$ (and anchors not aligned), a direct computation called trilateration is possible and will lead to an unique 2D position or 2 symmetrical 3D positions. Since in our case the anchors are placed on the ground, the horizontal plane is the symmetry plane and the negative altitude can be discarded.

- If $N \geq 4$ (and anchors not in the same plane), a solution of this multilateration problem can be computed by solving a linear system (as seen in [7]) either by a direct method when $M = 4$ (system is invertible) or with a minimization algorithm when $M > 4$.

Considering operational constraints, the case of multilateration is discarded since it requires, to be efficient, that at least one anchor is not placed in the ground plane. In practice, it means that it shall be placed accurately high enough on a fixed pole. This is not usually possible using the natural landmarks and the poles holding the net in the considered scenario are subject to oscillations, due to the wind in particular.

Thus, the trilateration problem is solved using the following formulas, based on Figure 5, starting with the equations of the spheres:

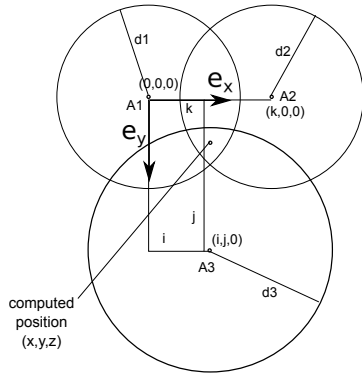$$\begin{aligned} d1^2 &= x^2 + y^2 + z^2 \\ d2^2 &= (x-k)^2 + y^2 + z^2 \\ d3^2 &= (x-i)^2 + (y-j)^2 + z^2 \end{aligned} \quad (1)$$

**IMAV2018-30**

http://www.imavs.org/pdf/imav.2018.30

10th International Micro-Air Vehicles Conference
22nd-23rd November 2018. Melbourne, Australia.

Figure 5: Trilateration problem parametrization.



Figure 6: Position errors with $d_{lat}$=5m and $d_{lon}$=5m.

After rewriting these equations, we have the following position estimate:

$$
\begin{array}{rcl}
x & = & \frac{d1^2 - d2^2 + k^2}{2k} \\
y & = & \frac{d1^2 - d3^2 + i^2 + j^2}{2j} - \frac{i}{j}x \\
z & = & \pm\sqrt{d1^2 - x^2 - y^2}
\end{array}
\quad (2)
$$

The final step is to compute the position $P$ in the original anchors' frame:

$$
P = P_{A1} + x\,\widetilde{e}_x + y\,\widetilde{e}_y + z\,\widetilde{e}_z \quad (3)
$$

where $P_{A1}$ is the original position of anchor 1, $\widetilde{e}_{[xyz]}$ are the base vectors for the trilateration projected into the original frame, and only the positive $z$ coordinate is kept.

### 3.3 Precision evaluation

The precision of the position computed with this method is evaluated using monte-carlo simulations. The Figure 6 shows the situation with separations of 5 meters for both $d_{lat}$ and $d_{lon}$. For each point of the graph, the theoretical measured distances are computed, then a gaussian white noise is added to the measures with the characteristics found during calibration (see section 3.1). Finally the standard deviation $\sigma$ of the resulting position errors (from 100 simulations) are used to evaluate the precision, assuming that 99% of the points will be in the range of $3\sigma$. The colors of the graph reflect this precision. In addition, the red line correspond to the desired landing path as described section 2.

The first observation is that the precision on the horizontal plane (here at a constant altitude of 20 meters) is about 10 times better than in the vertical plane, where the maximum errors can reach up to 16 meters at 80 meters of the final landing point. The reason for that is that the precision increases when the baseline between the anchors is increasing. On the horizontal plane, there is at least always a baseline of 5 meters in all directions due to the triangular shape of the anchors' locations (see Figure 2). On the vertical plane, because of the
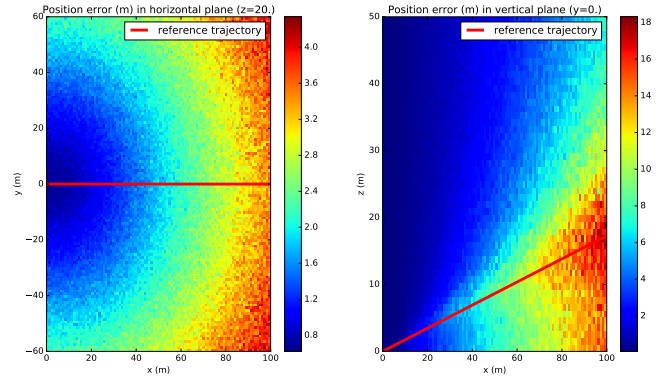
followed path, with a small angle of $10°$, the actual baseline is much reduced ($d_{lon} * sin(\gamma_{land})$ in this case).

In order to investigate the influence of the lateral and longitudinal separations of the anchors, a graph representing a normalized error score as a function of these two parameters is build. The score is evaluated as the sum of the standard deviation along the reference path:

$$
\text{score} = \sum_{\text{along reference path}} \sqrt{\sigma_x^2 + \sigma_y^2 + \sigma_z^2}
$$

The Figure 7 shows the resulting computation with the red lines corresponding to the frontier to have at least a score lower than 40%, 20% or 10% of the worst case.
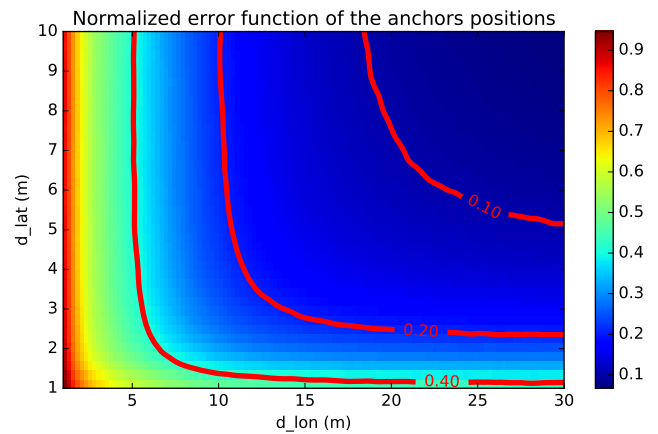


Figure 7: Normalized error score function of $d_{lat}$ and $d_{lon}$.

The conclusions of this graph are that the lateral distance $d_{lat}$ doesn't influence a lot above 5 meters, while an important value for $d_{lon}$ is required to reach a good overall precision. In fact, a longitudinal distance of 30 meters is needed to have similar results on all axis. This is again rising an operational issue that placing accurately the third anchors at a

**IMAV2018-30**

http://www.imavs.org/pdf/imav.2018.30

10th International Micro-Air Vehicles Conference
22nd-23rd November 2018. Melbourne, Australia.

long distance in front of the others is not easy to achieve and may decrease the final efficiency of the system. The same procedure applied to other anchors geometry have been considered. Placing the anchor 1 behind the net (negative values of $d_{lon}$) gives similar but slightly lower results. So this solution should be used only if the front position is not possible. Placing the same anchor 5 meters above the ground on top of anchors 2 (e.g. on top of one of the pole holding the net) gives excellent results in terms of precision but shall be discarded for now due to operational constraints as already stated in section 3.2.

For later analyzes, the parameters that will be chosen are 5 meters for both as an acceptable trade-off between precision and operational constraints.

## 4 EXPERIMENTAL FLIGHT ANALYZES

### 4.1 Experimental setup

Experimental flights have been performed in order to evaluate the performances of the positioning system in dynamic and long range conditions. The used aircraft is a foam based flying wing, equipped with the *Apogee* autopilot from the *Paparazzi UAV*[2] system [9]. The standard GPS receiver have been replaced by a *U-Blox M8P* differential GPS, with its ground base receiver, in order to have an accurate reference trajectory. The nominal airspeed for this plane is around 15 m/s. The Decawave *DW1000M* module used as tag is connected to the autopilot board through an *Arduino* performing the connection to the anchors and computing the distances. The complete setup is shown Figure 8.
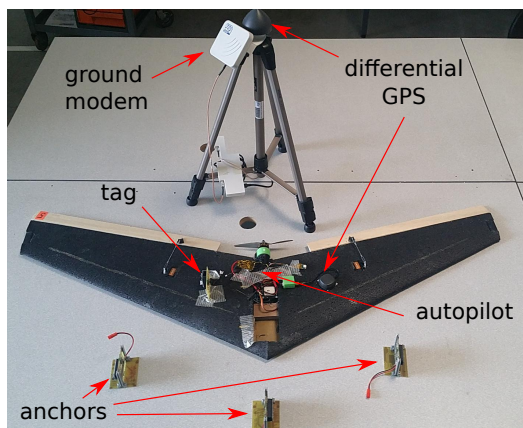


Figure 8: The experimental flying wing equipped with Decawave modules and DGPS system.

### 4.2 Direct computation limitations

The Figure 9 shows the distance reported by anchor 1 while the plane is flying over it about 20 meters above ground. Compared to the distance computed from the DGPS positions

---

[2]http://paparazziuav.org

after the flight, the correlation is good, but it can be noted that some wrong measurements can occur (at t=1140s) and some over are missing especially far from the anchor. The normal frequency during the flight with 3 anchors was 6.9 Hz. Also, during flights, the maximum range is usually shorter than static tests, with valid measures around 160 meters away, which is still acceptable for the landing procedure.
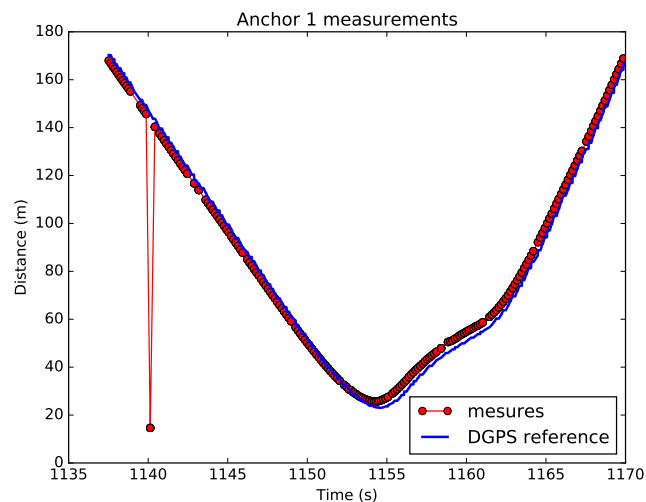


Figure 9: Measurements of anchor 1 compared to DGPS reference.

The main issue of the trilateration direct computation is that it makes the assumption that all three distances are available at the same time. This is not valid during dynamic flight, when the distances are retrieved in sequence while the plane is moving. With an airspeed of 15 m/s and landing in front of a 5 m/s wind speed as during flight test, the distance flown between two measures is about 1.5 meter, which is way above the 10 cm precision used during the static performance evaluation. This issue is illustrated by the Figure 10 showing many wrong position estimations. The reference trajectory coming from the DGPS and projected in the anchors' frame still show a good correlation except for the $z$ axis far from the anchors (at the beginning and the end of the plot).

### 4.3 Extended Kalman Filter for continuous correction

The solution to overcome the problem raised in the previous section is to perform a continuous integration of the data each time a new distance measurement is available. This is typically done with Kalman filters. Since the problem involves non-linear equations that are simple to derive, the most suited filter appears to be the Extended Kalman Filter (EKF), easier to implement than Unscented or Particle filters.

To implement such filter, the model is a second order kinematic model with constant velocity (the acceleration representing the command vector is always null) with position
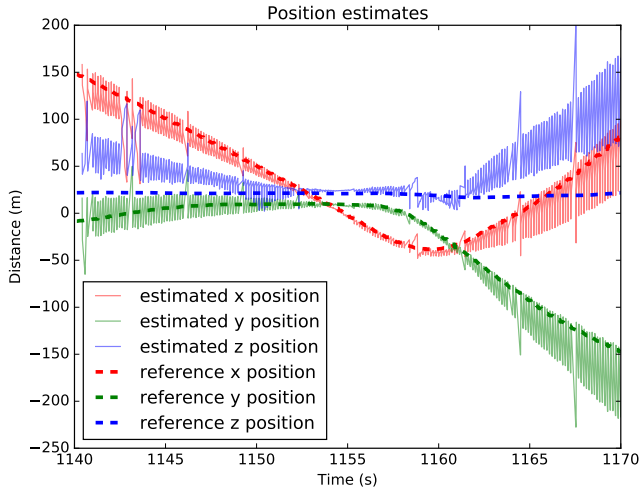
**IMAV2018-30**

http://www.imavs.org/pdf/imav.2018.30

10th International Micro-Air Vehicles Conference
22nd-23rd November 2018. Melbourne, Australia.

Figure 10: Estimated positions from direct computation.

and velocities as state vector elements:

$$\widehat{X}_k = \begin{bmatrix} x_k & y_k & z_k & vx_k & vy_k & vz_k \end{bmatrix}^T \quad (4)$$

In discrete time, the dynamic equation and covariance propagation are thus:

$$\widehat{X}_{k+1|k} = F_k \, \widehat{X}_k = \begin{bmatrix} 1 & 0 & 0 & T_e & 0 & 0 \\ 0 & 1 & 0 & 0 & T_e & 0 \\ 0 & 0 & 1 & 0 & 0 & T_e \\ 0 & 0 & 0 & 1 & 0 & 0 \\ 0 & 0 & 0 & 0 & 1 & 0 \\ 0 & 0 & 0 & 0 & 0 & 1 \end{bmatrix} \widehat{X}_k \quad (5)$$

$$P_{k+1|k} = F_k \, P_{k|k} \, F_k^T + Q_k \quad (6)$$

where $T_e$ is the sampling interval and $Q_k$ the process noise.

The observation model $h_i$ corresponds to the distance measurement from each anchor at position $[ax_i \; ay_i \; az_i]$ with $i \in \{1, 2, 3\}$. Then:

$$h_i(\widehat{X}_k) = \sqrt{(x_k - ax_i)^2 + (y_k - ay_i)^2 + (z_k - az_i)^2} \quad (7)$$

and its Jacobian is:

$$H_i(\widehat{X}_k) = \begin{bmatrix} \frac{x_k - ax_i}{\sqrt{(x_k - ax_i)^2 + (y_k - ay_i)^2 + (z_k - az_i)^2}} \\ \frac{y_k - ay_i}{\sqrt{(x_k - ax_i)^2 + (y_k - ay_i)^2 + (z_k - az_i)^2}} \\ \frac{z_k - az_i}{\sqrt{(x_k - ax_i)^2 + (y_k - ay_i)^2 + (z_k - az_i)^2}} \\ 0 \\ 0 \\ 0 \end{bmatrix}^T \quad (8)$$

Finally, at each new measurement $z_{i_k}$ from one of the anchors, we can apply to correction steps of the EKF:

$$K_k = P_{k+1|k} H_{i_k}^T (H_{i_k} P_{k+1|k} H_{i_k}^T + R_k)^{-1} \quad (9)$$

where $K_k$ is the Kalman gain and $R_k$ the measurement noise, and

$$\widehat{X}_{k+1|k+1} = \widehat{X}_{k+1|k} + K_k \left( z_{i_k} - h_i(\widehat{X}_{k+1|k}) \right) \quad (10)$$

$$P_{k+1|k+1} = (I - K_k H_{i_k}) P_{k+1|k} \quad (11)$$

update the state and covariance matrix. Note that this implementation only requires to compute the inverse of a scalar (and not a matrix) to compute the Kalman gain.

In order to have a correct and fast convergence of the EKF, it is necessary to initialize the filter with a state close to its true value. The idea is then to use a direct computation method (either trilateration or multilateration depending on the number of anchors) and then use the EKF to integrate subsequent measurements. The result of this process for the same set of data than Figure 10 is shown Figure 11.
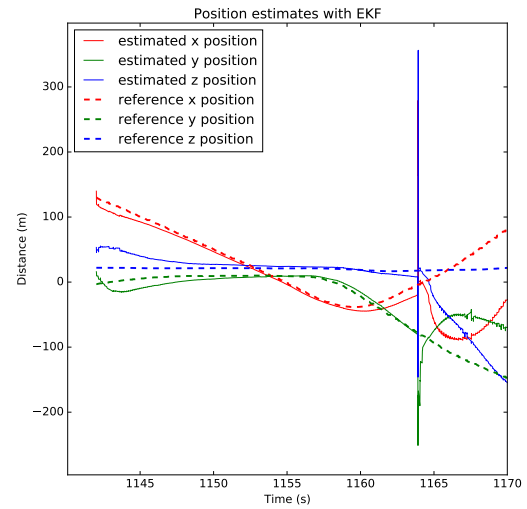


Figure 11: Estimated positions from Extended Kalman filter.

The estimated trajectory is smooth compared to the direct computation and converge to the reference trajectory, especially when the plane is flying towards the anchors (between 1140 and 1160 seconds). After that point, a combination of several effects (high bank angle of the plane while turning, faster speed due to tailwind and especially wrong measurement from an anchor) led to less accurate estimate and even stalling of the filter. It is thus required to implement a proper pre-filter to remove erroneous data, such as peak-removal or median filter.

Note that it is eventually possible to directly integrate the GPS speed norm to the filter as measurement, since the Earth and anchors frame are both fixed relative to the ground, even if their respective axis are different. This might improve the speed estimate of the filter.

**IMAV2018-30**

http://www.imavs.org/pdf/imav.2018.30

10th International Micro-Air Vehicles Conference
22nd-23rd November 2018. Melbourne, Australia.

### 4.4 Improving the dynamic model

The biggest issue that can be seen figure 11 is the latency in the position estimation when the aircraft is turning. This is coming from the constant speed assumption that is not valid during this phase. The result is that when closing the loop with the trajectory control to stay on the landing axis, this may lead to oscillating or even unstable trajectories. The improvement that can be made is to change the dynamic model to integrate the lateral acceleration as an input. When assuming a coordinated turn, it can be expressed as the product of the speed norm and the turn rate $\Omega$ (from attitude estimation filter) around the vertical axis.

$$\begin{cases} \dot{x} &= V_h\,cos(\psi) \\ \dot{y} &= V_h\,sin(\psi) \\ \dot{z} &= V_z \\ \dot{V_h} &= 0 \\ \dot{\psi} &= V_h\,\Omega \\ \dot{V_z} &= 0 \end{cases} \qquad (12)$$

With this modification and peak filtering, the resulting position estimation finally performs well even during the turn as seen figure 12. Some errors remain when the plane is flying away from the anchors.
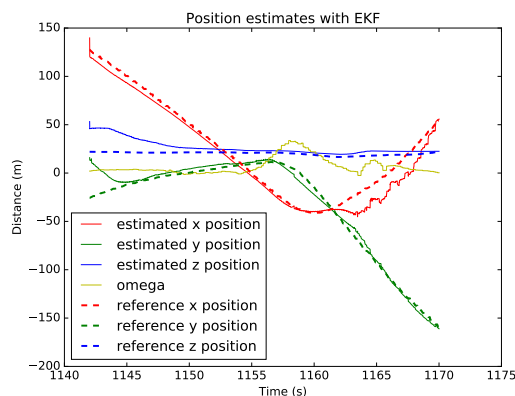


Figure 12: Position estimation with turn rate input.

## 5 CONCLUSION

In this article, we have presented an evaluation of the performances of a precision landing system for fixed wing mini-UAVs. The Ultra-Wide-Band technology is offering an easy way to deploy anchors and tags in order to provide accurate distance measurements, and it is compatible with the flight speed of this type of aircraft. Despite that, it is required to apply the correct combination of filters to efficiently estimate the position of the plane in the local anchors' frame. It also have been shown that the optimal location of the anchors are usually conflicting the operational constraints. This approach for local positioning can also be reused in various situations, like indoor flight or precision landing of rotorcraft UAVs.

## REFERENCES

[1] V. F. Vidal, L. M. Honrio, M. F. Santos, M. F. Silva, A. S. Cerqueira, and E. J. Oliveira. Uav vision aided positioning system for location and landing. In *2017 18th International Carpathian Control Conference (ICCC)*, pages 228–233, May 2017.

[2] Y. Lin, W. Lu, K. Chen, and J. Guo. Vision-based landing system design for a small uav. In *2015 IEEE International Conference on Consumer Electronics - Taiwan*, pages 496–497, June 2015.

[3] F. Lazzari, A. Buffi, P. Nepa, and S. Lazzari. Numerical investigation of an uwb localization technique for unmanned aerial vehicles in outdoor scenarios. *IEEE Sensors Journal*, 17(9):2896–2903, May 2017.

[4] W. Kong, D. Zhang, and J. Zhang. A ground-based multi-sensor system for autonomous landing of a fixed wing uav. In *2015 IEEE International Conference on Robotics and Biomimetics (ROBIO)*, pages 1303–1310, Dec 2015.

[5] H. Li, Z. Zhong, W. Kong, and D. Zhang. A fast calibration method for autonomous landing of uav with ground-based multisensory fusion system. In *2015 IEEE International Conference on Information and Automation*, pages 3068–3072, Aug 2015.

[6] J. Sidorenko, N. Scherer-Negenborn, M. Arens, and E. Michaelsen. Multilateration of the local position measurement. In *2016 International Conference on Indoor Positioning and Indoor Navigation (IPIN)*, pages 1–8, Oct 2016.

[7] J. Yang, H. Lee, and K. Moessner. Multilateration localization based on singular value decomposition for 3d indoor positioning. In *2016 International Conference on Indoor Positioning and Indoor Navigation (IPIN)*, pages 1–8, Oct 2016.

[8] Garapati kesava harinath and J. Ravi kumar. Implementation and performance evolution of kalman filters for target tracking using bistatic range and range rate measurements. In *2014 International Conference on Electronics and Communication Systems (ICECS)*, pages 1–5, Feb 2014.

[9] Gautier Hattenberger, Murat Bronz, and Michel Gorraz. Using the Paparazzi UAV System for Scientific Research. In *IMAV 2014, International Micro Air Vehicle Conference and Competition 2014*, pages pp 247–252, Delft, Netherlands, August 2014.